

1 **Title:**

2 **Atlantic Induced Pan-tropical Climate Change over the Past Three Decades**

3

4 **Author information:**

5 **Author**

6 Xichen Li^{1*}, Shang-Ping Xie^{1*}, Sarah T. Gille¹ & Changhyun Yoo².

7

8 **Affiliations:**

9 ¹Scripps Institution of Oceanography, University of California, San Diego, USA.

10 ²Department of Atmospheric Science and Engineering, Ewha Womans University, Seoul,

11 Republic of Korea.

12 *Corresponding author

13

14 **Contact Information:**

15 Xichen Li: xichenslc@gmail.com

16 Shang-Ping Xie: sxie@ucsd.edu

17 Sarah Gille: sgille@ucsd.edu

18 Changhyun Yoo: cyoo@ewha.ac.kr

19

19 **Summary**

20 During the last three decades, tropical sea surface temperature (SST) has shown dipole-
21 like trends, with warming over the tropical Atlantic and Indo-Western Pacific but cooling
22 over the Eastern Pacific. Competing hypotheses relate this cooling, identified as a driver
23 of the global warming hiatus^{1,2}, to the warming trends in either the Atlantic^{3,4} or Indian
24 Ocean⁵. However, the mechanisms, the relative importance, and the interactions between
25 these teleconnections remain unclear. Using a state-of-the-art climate model, we show
26 that the Atlantic plays a key role in initiating the tropical-wide teleconnection, and the
27 Atlantic-induced anomalies contribute ~55%-75% of the tropical SST and circulation
28 changes during the satellite era. The Atlantic warming drives easterly wind anomalies
29 over the Indo-Western Pacific through the Kelvin wave, and westerly anomalies over the
30 eastern Pacific as Rossby waves. The wind changes induce an Indo-Western Pacific
31 warming via the wind-evaporation-SST effect^{6,7}, and this warming intensifies the La
32 Niña-type response in the tropical Pacific by enhancing the easterly trade winds and
33 through the Bjerknes ocean-dynamical processes⁸. The teleconnection develops into a
34 tropical-wide SST dipole pattern. This mechanism, supported by observations and a
35 hierarchy of climate models, reveals that the tropical ocean basins are more tightly
36 connected than previously thought.

37

37 The tropics have experienced marked climate change since 1979 when the era of
38 global satellite observations began. Sea surface temperature (SST) trends exhibit a pan-
39 tropical dipole-like pattern (**Fig. 1a**), with extensive warming from the tropical Atlantic
40 to the Indo-Western Pacific, and a triangular cooling pattern in the Central-Eastern
41 Pacific. This tropical-wide gradient in the SST trend interacts with the atmospheric and
42 oceanic circulation throughout the tropics (**Fig. 1c, e**), with an enhanced Walker
43 circulation⁹⁻¹¹ and a La-Niña-like Pacific sub-surface response. These changes further
44 contribute to global climate change^{1,12,13} via multiple atmospheric teleconnections^{8,14}.

45 The tropical ocean basins are connected through atmospheric bridge¹⁵ into an
46 interactive system. On interannual time scales, El Niño-Southern Oscillation (ENSO)
47 dominates the tropical inter-basin teleconnections^{15,16}, although the Indian^{17,18} and
48 Atlantic¹⁹⁻²¹ Oceans experience regional effects that can feedback to the Pacific. In this
49 inter-basin teleconnection, El-Niño warming heats the Indian and Atlantic basins¹³. Were
50 the same relationship to hold on multidecadal time scales, the cooling of the Eastern
51 Pacific would be linked to decreased SSTs in the Indian and Atlantic basins
52 (**Supplementary Fig. 1**), contrary to the observed trends. This discrepancy implies that
53 other mechanisms are required to compensate the Eastern Pacific induced tropical
54 cooling.

55 The north and tropical Atlantic has experienced a continuous warming trend, due
56 to the combined effects of anthropogenic radiative forcing^{7,22} and the change in
57 Meridional Overturning Circulation^{23,24}. Pioneering work using slab ocean-atmospheric
58 models³ and reduced-gravity ocean-atmospheric models⁴ suggest that this observed
59 Atlantic warming directly contributes to the Eastern Pacific cooling, although the full
60 range of ocean dynamics and atmospheric-ocean interactions may not be well represented
61 by these idealized oceanic models. Here we simulate the global impact of the tropical

62 Atlantic warming using a fully coupled earth system model, and further investigate the
63 mechanisms of these teleconnections using a hierarchy of climate models. The results
64 from the coupled model show that the Atlantic warming can induce a basin-scale
65 warming over the Indian Ocean and Western Pacific through atmospheric bridge. This
66 secondary Indo-Western Pacific warming, together with the original Atlantic warming,
67 intensifies the easterly wind anomaly over the Pacific, accelerates the Walker circulation,
68 and contributes to the La-Niña-type response over the Pacific (**Fig. 1**). Both surface heat
69 fluxes and ocean dynamics play key roles in this tropical-wide pattern formation.

70 We first test the hypothesis that the tropical Atlantic warming drives the tropical-
71 wide change by nudging the tropical Atlantic SST in a state-of-the-art fully coupled
72 model (**Fig. 1b**), the Community Earth System Model (CESM1, see Method Section).
73 The restoring reproduces the bulk of the observed warming trend over the tropical
74 Atlantic (97%, see gray bars in **Supplementary Fig. 2c**). Forced by this Atlantic
75 warming, the model (**Fig. 1b**) captures the detailed features of the observed tropical-wide
76 SST changes (**Fig. 1a**), i.e., a significant warming anomaly over the Indo-Western Pacific
77 (**Supplementary Fig. 2c** blue bars), and significant cooling anomalies in the off-
78 equatorial Eastern Pacific (purple and green bars). A Mann-Kendall test indicates that the
79 observed equatorial Pacific cooling trend from 1979 to 2013 is only marginally
80 significant (left red bar) due to high internal variability and the short period. With a large
81 sample size, the Pacific cooling is significant in the ensemble simulation with a Student t -
82 test. In addition, the 25-year-mean results for each of the 12 ensemble members
83 (**Supplementary Fig. 2c**) show a cooled equatorial eastern Pacific in response to the
84 Atlantic warming, indicating a robust anti-correlated relationship between these two
85 ocean basins. The coupled simulation captures 55% - 75% of the observed trends over the
86 Indian and Pacific Oceans, highlighting the association between the Atlantic warming

87 and pan-tropical SST changes, although additional mechanisms, e.g. anthropogenic
88 radiative forcing for the Indo-Western Pacific warming⁷, are likely required to explain the
89 entire observed SST trend.

90 The Atlantic warming induced tropical-wide SST pattern drives a series of
91 tropical climate changes in the CESM (**Fig. 1** right panels). The enhanced convection
92 forced by the surface warming heats the troposphere, and the deep convection over the
93 Indo-Western Pacific warm pool area intensifies the Indo-Pacific Walker circulation (**Fig.**
94 **1c, d**). At the surface, this circulation change manifests itself as a strengthened easterly
95 wind anomaly¹¹ over the equatorial Pacific (**Fig. 1a**). With the dynamical ocean-
96 atmosphere coupling, this simulated equatorial Pacific easterly wind anomaly captures
97 68% of the observed trend (**Supplementary Fig. 2c**), albeit with a slight westward shift
98 (**Fig. 1b**). This wind anomaly is accompanied by a La-Niña-like Pacific subsurface
99 anomaly both in observations and in the simulation (**Fig. 1e,f**). The coupled model
100 successfully captures the main features of the observed temperature and circulation
101 changes over the tropical ocean and atmosphere, although some of the detailed
102 characteristics are not fully reproduced. In particular, the observed atmospheric
103 temperature has exhibited a cooling trend over the African continent (**Fig. 1b**), associated
104 with a downwelling flow in the troposphere. This is not well represented by the
105 simulation, indicating that land-air interaction may be important for understanding the
106 changes over that region. Additionally, the simulated atmospheric vertical motion (**Fig.**
107 **1d**) is both weaker and more widespread than the observed changes (**Fig. 1c**), which may
108 be related to the convective scheme in the atmospheric model.

109 To better identify the potential sources of the pan-tropical climate variability (**Fig.**
110 **1a**), we also nudge the SST changes over the Indian Ocean and the Pacific Ocean,
111 separately. The Indian Ocean nudging replicates the observed cooling trend in the Eastern

112 Pacific¹, albeit with a smaller amplitude, but it erroneously cools the Atlantic
113 (**Supplementary Fig. 3**). The Pacific nudging, on the other hand, cools the Indian Ocean.
114 Both simulations produce an SST response that is partially inconsistent with
115 observations, indicating that the Atlantic is the most consistent driver of the pan-tropical
116 dipole-like SST variability.

117 While our Atlantic nudging simulations successfully reproduce the observed
118 trends, the coupled model alone does not reveal the mechanisms underlying these pan-
119 tropical inter-basin teleconnections. Next, we use an idealized atmospheric model and a
120 comprehensive atmospheric model to identify the dynamical pathways by which the
121 tropical Atlantic warming forces the tropical-wide climate changes.

122 CESM simulations involve both atmospheric dynamics and atmosphere-ocean
123 interactions. To single out the immediate atmospheric responses to the Atlantic SST
124 forcing, we introduce a tropical Atlantic heating to an idealized atmospheric model – the
125 dry-dynamical-core of the GFDL atmospheric model (Methods). The atmospheric deep
126 convection generated by the Atlantic warming (**Supplementary Fig. 4**) excites an
127 equatorial Kelvin-wave, inducing strong easterly wind anomalies to the east of the SST
128 forcing (**Supplementary Fig. 5b**), as well as two Rossby wave packets with equatorial
129 westerly wind anomalies and two off-equatorial cyclonic flows, west of the heat source.
130 This circulation pattern closely resembles the classic Gill-model²⁵. Within one week, the
131 Kelvin-wave induced easterly wind anomalies extend from the Atlantic Ocean to the
132 international-date-line (**Supplementary Fig. 5c**), traversing the entire Indian Ocean and
133 Western Pacific, while the Rossby-wave equatorial westerly wind anomalies occupy the
134 Eastern Pacific and Central America.

135 Moisture processes are important in the tropics but are absent in the GFDL-dry-
136 dynamical-core. The Community Atmospheric Model (CAM4, Methods) is the
137 atmospheric component of CESM1 and includes interactive moist processes. The CAM4
138 response agrees well with that of the idealized simulation (**Supplementary Fig. 5c,d**),
139 again showing an easterly wind anomaly extending from the Atlantic to the Indo-Western
140 Pacific and a westerly wind anomaly over the Eastern Pacific. The Kelvin-wave induced
141 easterly wind anomalies favor a La-Niña-type ocean dynamical response⁸, consistent with
142 the coupled model results. In contrast, the Rossby-wave induced westerly wind anomalies
143 favor an El-Niño-type response.

144 To investigate the direct ocean response to these atmospheric circulation
145 anomalies, we use the anomalies to force an ocean-only model (POP2, see
146 **Supplementary Fig. 6**). In the absence of ocean-atmosphere feedbacks, the ocean model
147 response is different from the La-Niña-type responses simulated in the fully-coupled
148 model. This discrepancy highlights the importance of atmosphere-ocean interactions in
149 the pan-tropical teleconnections. The remainder of this work investigates atmosphere-
150 ocean interactions that further enhance the equatorial Pacific easterly wind anomalies and
151 the Walker circulation, thus contributing to a La-Niña-like Pacific response.

152 Atmospheric forcing may influence regional SST by changing surface heat flux
153 and oceanic dynamical effects^{6,7}. In CAM4, the surface energy-exchanges over the Indo-
154 Pacific oceans are dominated by the wind-induced latent heat flux (**Fig. 2b**), whose
155 contribution is ~3 times greater than that of all the other components of surface heat flux
156 combined (**Supplementary Fig. 7**). The Kelvin-wave induced easterly wind anomaly
157 over the Indian Ocean reduces surface wind speed (blue contours in **Fig. 2b**) and
158 suppresses evaporation, which warms the Equatorial-Northern Indian Ocean (red color in
159 **Fig. 2b**) via the wind-evaporation-SST effect⁶ (WES, Methods). Note that in the

160 atmosphere-only simulation (**Fig. 2b**), the SSTs are fixed and cannot feed back to the
161 atmospheric circulation. The simulated regional-mean latent heat flux anomaly is ~ 4.35
162 W/m^2 , corresponding to an initial heating rate of the ocean mixed layer of ~ 0.05
163 K/month , which implies a fast response of Indo-Western Pacific with a time scale of ~ 1
164 year. This fast response is well reproduced in the coupled model and is supported by the
165 statistical analyses of the observational data and the CMIP5 simulations (**Supplementary**
166 **Fig. 8**)

167 To the west of the Atlantic warming, the Rossby-wave-induced circulation
168 changes strengthen the trade winds and cool the off-equatorial Eastern Pacific in both
169 hemispheres (blue color in **Fig. 2b**). This cooling signal may propagate equatorward and
170 westward to the central-equatorial Pacific via the WES seasonal footprinting
171 mechanism²⁶. The Kelvin-wave-induced easterly wind anomaly also cools the central
172 equatorial Pacific around the international dateline. These WES cooling effects contribute
173 to an SST decrease over the Central-Eastern Pacific, which has been well simulated by a
174 recent study using a slab ocean-atmosphere coupled model³.

175 The Atlantic-induced Indo-Western Pacific warming generates a secondary
176 atmospheric deep convection (**Fig. 2c**, also see **Supplementary Fig. 9**) with westerly
177 wind anomalies over the Indian Ocean, and an easterly wind anomaly across the Pacific
178 basin. This secondary circulation change, representing an enhanced Indo-Pacific Walker
179 circulation, explains the different atmospheric circulation responses between the CAM4
180 and CESM results. It reinforces the Atlantic-induced easterly wind anomalies over the
181 western equatorial Pacific, overwhelming the Atlantic-induced westerly wind anomalies
182 over the eastern equatorial Pacific. Atmospheric circulation changes further interact with
183 Pacific Ocean dynamics through the Bjerknes feedback^{4,8}. This feedback is at work in the
184 coupled model (**Fig. 2d**): over the equatorial Pacific strong easterly winds drive an

185 enhanced SST gradient, which further intensify the winds, ultimately giving rise to a La-
186 Niña-like subsurface anomaly in the Pacific Ocean. In contrast, the ocean dynamical
187 response is comparatively weak in the Indian Ocean, which experiences an overall
188 warming in the upper 300m with a cooling at ~100m (**Fig. 1e**). The Indian Ocean
189 temperature change is primarily a direct response to the surface heat fluxes, while the
190 Indonesian Throughflow may also contribute to these upper layer changes²⁷.

191 In summary, we have shown that the tropical Atlantic warming over the past three
192 decades, aided by coupled ocean-atmosphere processes, caused a tropical-wide response
193 that included the Indo-Western Pacific warming and eastern Pacific cooling. The direct
194 atmospheric response to the tropical Atlantic warming includes easterly wind anomalies
195 over the Indo-Western Pacific in the form of Kelvin waves, and westerly wind anomalies
196 over the eastern equatorial Pacific as Rossby waves (**Fig. 3a**), in line with Gill's solution.
197 The easterly wind anomalies cause the Indo-Western Pacific to warm and the central
198 equatorial Pacific to cool through the WES effect, while the Rossby wave gyres intensify
199 the easterly trade winds in the off-equatorial Eastern Pacific, contributing to the
200 equatorial Pacific cooling via the WES foot-printing mechanism (**Fig. 3a**). This surface
201 atmospheric-ocean interaction generates a temperature gradient over the Indo-Pacific
202 basins, which further enhances the Walker circulation and induces easterly wind
203 anomalies across the equatorial Pacific, and drives it into a La-Niña state (**Fig. 3b**). The
204 Bjerknes feedback helps amplify the coupling of the equatorial Pacific cooling and
205 easterly intensification.

206 A global SST pattern characterized by the eastern Pacific cooling and warming
207 over the rest of oceans is identified as the most predictable mode at multi-year lead
208 times²⁸. Pacific decadal variability may be partly tied to Atlantic multidecadal
209 oscillation^{29,30}. The tropical Atlantic warming trend is likely due to radiative forcing^{7,22}

210 and Atlantic Multi-decadal Oscillation^{23,24}, the latter possibly tied to the Atlantic
211 meridional overturning circulation (AMOC). The mechanism revealed by this study
212 suggests that the AMOC may force the pan-tropical decadal variability, and the slow time
213 scales of the AMOC may explain the decadal predictability^{19,28} of the tropical-wide SST
214 pattern.

215 The Indo-Western Pacific SST response to the tropical Atlantic warming is almost
216 immediate, with a timescale of ~1 year. In contrast, there exists a ~10 year phase lag
217 between the Atlantic warming and the cooling phase of the Pacific Decadal Oscillation³⁰.
218 This decadal-scale phase lag may be related to shorter-term variability such as ENSO,
219 which serves as a stochastic forcing to the long-term variability. In this study we mainly
220 focus on explaining the observed trend during the satellite era, but we plan to address this
221 phase-lag problem in future work. Additionally, our coupled simulations are forced by a
222 fixed radiative forcing. The radiative forcing changes caused by increased greenhouse
223 gases could further warm the Atlantic Ocean and the Indo-Western Pacific, although its
224 impact on the Eastern Pacific requires further investigations.

225 While recent studies of the global warming hiatus have focused on the Pacific
226 effect¹, consistent with earlier studies²⁻⁴ our results suggest that the hiatus may ultimately
227 be traced back to the warming in tropical Atlantic. This teleconnection is aided by Indo-
228 Western Pacific adjustments as revealed in this study. Together, these studies show that
229 the three tropical ocean basins are linked more closely than previously thought, and on
230 decadal time scales the tropical oceans should be considered as a single entity. In addition
231 to the well-known ENSO-induced tropical-wide response that is dominant on inter-annual
232 time scales, this study highlights the role of the tropical Atlantic in initiating a different
233 pan-tropical dipole pattern that is important on decadal timescales.

234 **Online Methods**

235 **Data sets.** The UK Met Office Hadley Centre's SST dataset HadISST³¹ was employed in
236 this study to estimate the trend of the Tropical SST from 1979 to 2012 (**Fig. 1a**), and the
237 SST trend over the Tropical Atlantic estimated by this dataset was used to force the
238 CESM and CAM4 models. The Kaplan Extended SST version2³², and the National
239 Oceanic and Atmospheric Administration (NOAA) Extended Reconstructed SST version
240 3b³³, were also used together with the HadISST to reveal the decadal relationship
241 between the Tropical Atlantic and the Indo-Western Pacific.

242 The Ishii Subsurface Ocean Temperature Analysis³⁴ was used to calculate the
243 subsurface ocean temperature trends from 1979 to 2012 (**Fig. 1e**). The Global
244 Precipitation Climatology Project³⁵ (GPCP) data were used to estimate the trend in the
245 tropical precipitation for the same period. The European Centre for Medium Range
246 Weather Forecasts (ECMWF) Interim Re-Analysis³⁶ (ERA-Interim) data were used to
247 estimate the trend in the atmospheric circulation (**Fig. 1a,c**).

248 Model results from the Coupled Model Intercomparison Project³⁷ (CMIP5)
249 historical experiments were used to identify the relationship between the Tropical
250 Atlantic and the Indo-Western Pacific decadal-mean SST.

251

252 **Analyses methods.** Sen's slope³⁸ method is used to calculate the observed trends, with
253 the confidence intervals estimated using the Mann-Kendall test³⁹. We used Student's *t*-
254 test to calculate the confidence interval of the model responses.

255

256 **CESM model experiments.** The National Center for Atmospheric Research (NCAR)
257 coupled climate model, the Community Earth System Model⁴⁰ (CESM1.06) was used in
258 this study to investigate the response of the tropical climate system to an observed
259 Tropical Atlantic warming. We used F19_G16⁴⁰ horizontal resolution, with ~2 degree
260 resolution in the atmospheric component, and ~1 degree in the ocean component. We
261 restored the Tropical Atlantic temperature in the coupled model with an external heating
262 within the mixed layer as follows:

$$263 \quad F = cD(T_r - T_m) / \tau$$

264 Where c is the heat content of sea water, D is the mixed layer depth, T_r is the restoring
265 target temperature, T_m is the model temperature at each time step, and τ is the restoring
266 time scale, which was set as 20 days in this study.

267 The CESM response to the Tropical Atlantic warming was calculated as the
268 ensemble mean of 12 sensitivity experiments. In each experiment, we estimate the
269 difference between a control run and a perturbed run. In the control run, the ocean
270 temperature in the mixed layer of the tropical Atlantic (defined as the Atlantic Ocean
271 between 20°S and 20°N, with linear buffer zones extending from 20°S to 30°S and from
272 20°N to 30°N) was restored to the model climatology. In the perturbed run, the Tropical
273 Atlantic SST was restored to the model climatology plus the observed 1979-2012 SST
274 trend. We generated 12 ensemble members by slightly perturbing the external forcing
275 around the observed SST trend ($\pm 0.1\%$, $\pm 0.2\%$, $\pm 0.6\%$, $\pm 1\%$, $\pm 1.4\%$, $\pm 1.8\%$ from the
276 observed trend.) Each simulation starts from the year-2000 initial condition of the CESM
277 system and lasts for 30 model years. The first 5 years serve as a spin up simulation while
278 the results from year 6 to year 30 are used in the calculation. The ensemble mean of these

279 simulations is then considered to be the CESM response to the observed trend of the
280 Tropical Atlantic SST.

281

282 **CAM4 model simulations.** The NCAR atmospheric model, the Community Atmosphere
283 Model version 4 (CAM4), was used in this study to identify the tropical atmospheric
284 responses to the Atlantic SST trend from 1979 to 2012. CAM4 is the atmospheric
285 component of CESM and is run with the same resolution. As we do with the CESM
286 simulation, we estimate the CAM4 response by differencing the control runs (with the
287 climatological SST forcing) from the perturbed runs (forced by the Tropical Atlantic SST
288 trend).

289

290 **GFDL dry-dynamical-core simulations.** The spectral dry-dynamical-core of an
291 atmospheric general circulation model⁴¹, developed at the Geophysical Fluid Dynamics
292 Laboratory (GFDL), was used to investigate the evolution of the atmospheric response to
293 a tropical Atlantic warming, in a primitive-equation dynamical-system. The idealized
294 model is initialized with the climatological background flow from the ERA-interim
295 reanalysis, averaged from 1979 to 2012. At each time step, an additional forcing that
296 balances the model's initial tendency associated with the climatological background flow
297 was added to keep the model steady^{42,43}. This external forcing ensures that the model
298 response at each time step is due only to the initial tropical perturbation. In the forced
299 cases, a convective heating is added as an initial impulse over the tropical Atlantic. The
300 model results at each snapshot could be interpreted as the evolution of the primitive -
301 equation - dynamics in response to the tropical heating (see Yoo et al. 2012 for details).

302

303 **Surface heat flux and WES effect.** The change of SST $\partial T'/\partial t$ satisfies a balance^{5,6}
304 between the oceanic dynamics D_o and four surface heat flux components: solar radiation
305 Q_s , long wave radiation Q_L , sensitive heat flux Q_H , and latent heat flux Q_E , which can
306 be expressed as:

307
$$C \frac{\partial T'}{\partial t} = D_o + Q_s + Q_L + Q_H + Q_E$$

308 where C is the heat capacity of the upper ocean, up to the depth of interest.

309 The latent heat flux Q_E can be further decomposed into an atmospheric forcing
310 term Q'_E and an oceanic response term Q''_E ,

311
$$Q_E = Q'_E + Q''_E = \frac{\partial Q_E}{\partial W} W' + Q'_E + \frac{\partial Q_E}{\partial T} T'$$

312 The former is mostly sensitive to the surface wind anomaly (W'), and the latter serves as
313 a Newtonian damping with respect to the ocean temperature change (T'). Q'_E refers to
314 the residuals of the atmospheric forcing related to the relative humidity and stability
315 effect and serves as a second-order factor⁶ in this study.

316 When the surface wind is reduced, according to the bulk formula, the evaporation
317 will be suppressed. This effect thus increases the latent heat flux from the atmosphere to
318 the ocean, warming the sea surface⁵.

319

319 **References**

- 320 1. Kosaka, Y., & Xie, S. P. Recent global-warming hiatus tied to equatorial Pacific
321 surface cooling. *Nature* **501**, 403-407 (2013).
- 322 2. Meehl, G. A., et al. Model-based evidence of deep-ocean heat uptake during surface-
323 temperature hiatus periods. *Nature Clim Change*, **1**, 360-364 (2011).
- 324 3. McGregor, S., Timmermann, A., Stuecker, M. F., England, M. H., Merrifield, M., Jin,
325 F. F., & Chikamoto, Y. Recent Walker circulation strengthening and Pacific cooling
326 amplified by Atlantic warming. *Nature Clim. Change* **4**, 888-892 (2014).
- 327 4. Kucharski, Fred, I - S. Kang, Riccardo Farneti, and Laura Feudale. "Tropical Pacific
328 response to 20th century Atlantic warming." *Geophys. Res. Lett.* **38**, no. 3 (2011).
- 329 5. Luo, J. J., Sasaki, W., & Masumoto, Y. Indian Ocean warming modulates Pacific
330 climate change. *Proc. Natl. Acad. Sci.* **109**, 18701-18706 (2012).
- 331 6. Xie, S. P., & Philander, S. G. H. A coupled ocean-atmosphere model of relevance to
332 the ITCZ in the eastern Pacific. *Tellus A* **46**, 340-350 (1994).
- 333 7. Xie, S. P., Deser, C., Vecchi, G. A., Ma, J., Teng, H., & Wittenberg, A. T. Global
334 warming pattern formation: sea surface temperature and rainfall*. *J. Clim.* **23**, 966-
335 986 (2010)
- 336 8. Bjerknes, J. Atmospheric teleconnections from the equatorial pacific 1. *Monthly*
337 *Weather Review* **97**, 163-172 (1969).
- 338 9. Wang, Chunzai. An overlooked feature of tropical climate: Inter - Pacific - Atlantic
339 variability. *Geophys. Res. Lett.* **33**, no. 12 (2006).

- 340 10. Rodríguez - Fonseca, Belén, Irene Polo, Javier García - Serrano, Teresa Losada, Elsa
341 Mohino, Carlos Roberto Mechoso, and Fred Kucharski. Are Atlantic Niños
342 enhancing Pacific ENSO events in recent decades?. *Geophys. Res. Lett.* **36**, no. 20
343 (2009).
- 344 11. England, M. et al. Recent intensification of wind-driven circulation in the Pacific and
345 the ongoing warming hiatus. *Nature Clim. Change*, **4**, 222–227 (2014).
- 346 12. Li, X., Holland, D. M., Gerber, E. P., & Yoo, C. Impacts of the north and tropical
347 Atlantic Ocean on the Antarctic Peninsula and sea ice. *Nature* **505**, 538-542 (2014).
- 348 13. Lau, N. C., & Nath, M. J. A modeling study of the relative roles of tropical and
349 extratropical SST anomalies in the variability of the global atmosphere-ocean system.
350 *J. Clim.* **7**, 1184-1207 (1994).
- 351 14. Wallace, J. M., & Gutzler, D. S. Teleconnections in the geopotential height field
352 during the Northern Hemisphere winter. *Mon. Weather Rev.* **109**, 784-812 (1981).
- 353 15. Alexander, M. A., Bladé, I., Newman, M., Lanzante, J. R., Lau, N. C., & Scott, J. D.
354 The atmospheric bridge: The influence of ENSO teleconnections on air-sea
355 interaction over the global oceans. *J. Clim.* **15**, 2205-2231 (2002).
- 356 16. Chang, P., Fang, Y., Saravanan, R., Ji, L., & Seidel, H. The cause of the fragile
357 relationship between the Pacific El Niño and the Atlantic Niño. *Nature* **443**, 324-328
358 (2006).
- 359 17. Annamalai, H. S. P. X., Xie, S. P., McCreary, J. P., & Murtugudde, R. Impact of
360 Indian Ocean sea surface temperature on developing El Niño*. *J. Clim.* **18**, 302-319
361 (2005).

- 362 18. Kug, J. S., Kirtman, B. P., & Kang, I. S. Interactive feedback between ENSO and the
363 Indian Ocean in an interactive ensemble coupled model. *J. Clim.* **19**, 6371-6381
364 (2006).
- 365 19. Keenlyside, N. S., Latif, M., Jungclaus, J., Kornblueh, L., & Roeckner, E. Advancing
366 decadal-scale climate prediction in the North Atlantic sector. *Nature* **453**, 84-88
367 (2008).
- 368 20. Ham, Y. G., Kug, J. S., Park, J. Y., & Jin, F. F. Sea surface temperature in the north
369 tropical Atlantic as a trigger for El Niño/Southern Oscillation events. *Nature Geosci.*
370 **6**, 112-116 (2013).
- 371 21. Kucharski, F., F. S. Syed, A. Burhan, I. Farah, and A. Gohar. Tropical Atlantic
372 influence on Pacific variability and mean state in the twentieth century in
373 observations and CMIP5. *Climate Dynamics* **44**, 881-896 (2015).
- 374 22. Booth, B. B., Dunstone, N. J., Halloran, P. R., Andrews, T. & Bellouin, N. Aerosols
375 implicated as a prime driver of twentieth-century North Atlantic climate variability.
376 *Nature* **484**, 228–232 (2012).
- 377 23. Schlesinger, M. E., and Ramankutty, N. An oscillation in the global climate system of
378 period 65-70 years, *Nature*, **367**, 723-726 (1994).
- 379 24. Zhang, R, and Delworth. T. L. A new method for attributing climate variations over
380 the Atlantic Hurricane Basin's main development region. *Geophys. Res. Lett.*, **36**,
381 L06701 (2009).
- 382 25. Gill, A. Some simple solutions for heat-induced tropical circulation. *Q. J. Roy.*
383 *Meteor. Soc.* **106**, 447-462 (1980).

- 384 26. Vimont, D. J., Battisti, D. S., & Hirst, A. C. Footprinting: A seasonal connection
385 between the tropics and mid-latitudes. *Geophys. Res. Lett.* **28**, 3923-3926 (2001).
- 386 27. Lee, Sang-Ki, Wonsun Park, Molly O. Baringer, Arnold L. Gordon, Bruce Huber, and
387 Yanyun Liu. Pacific origin of the abrupt increase in Indian Ocean heat content during
388 the warming hiatus. *Nature Geosci.* **8** 445-449 (2015).
- 389 28. Chikamoto, Y., Timmermann, A., Luo, J. J., Mochizuki, T., Kimoto, M., Watanabe,
390 M., ... & Jin, F. F. Skilful multi-year predictions of tropical trans-basin climate
391 variability. *Nature communications*, **6** (2015).
- 392 29. Kucharski, F., Ikram, F., Molteni, F., Farneti, R., Kang, I., No, H., ... & Mogensen, K.
393 Atlantic forcing of Pacific decadal variability, *Climate Dynamics*, doi:
394 10.1007/s00382-015-2705-z (2015)
- 395 30. Zhang, R., & Delworth, T. L. Impact of the Atlantic multidecadal oscillation on
396 North Pacific climate variability. *Geophys. Res. Lett.* **33**, L17712 (2006).
- 397
- 398
- 399
- 400

400 **References in Online Methods**

- 401 31. Rayner, N. A. et al. Global analyses of sea surface temperature, sea ice, and night
402 marine air temperature since the late nineteenth century. *J. Geophys. Res.* **108**, 4407
403 (2003).
- 404 32. Kaplan, A., Cane, M. A., Kushnir, Y., Clement, A. C., Blumenthal, M. B., &
405 Rajagopalan, B. Analyses of global sea surface temperature 1856-1991, *J. Geophys.*
406 *Res.*, **103**, 18,567-18,589 (1998).
- 407 33. Smith, T.M., and Reynolds, R. W. Extended Reconstruction of Global Sea Surface
408 Temperatures Based on COADS Data (1854-1997). *J. Clim.*, **16**, 1495-1510 (2003).
- 409 34. Ishii, M., Kimoto, M., Sakamoto, K., & Iwasaki, S. I. Steric sea level changes
410 estimated from historical ocean subsurface temperature and salinity analyses. *J.*
411 *Oceanogr.*, **62**, 155-170 (2006).
- 412 35. Xie, P. et al. GPCP pentad precipitation analyses: An experimental dataset based on
413 gauge observations and satellite estimates. *J. Clim.* **16**, 2197-2214 (2003).
- 414 36. Dee, D. P. et al. The ERA-Interimreanalysis: configuration and performance of the
415 data assimilation system. *Q. J. R. Meteorol. Soc.*, **137**, 553–597 (2011).
- 416 37. WCRP Coupled Model Intercomparison Project – Phase 5: Special Issue of the
417 CLIVAR Exchanges Newsletter, No. 56, Vol. **15**, No. 2
- 418 38. Sen, P. K. Estimates of the regression coefficient based on Kendall’s tau. *J. Am. Stat.*
419 *Assoc.* **63**, 1379–1389 (1968).
- 420 39. Richard O. Gilbert. Statistical methods for environmental pollution monitoring. John
421 Wiley & Sons (1987).

- 422 40. Bretherton, C. S., Smith, C. & Wallace, J. M. An intercomparison of methods for
423 finding coupled patterns in climate data. *J. Clim.*, **5**, 541–560 (1992).
- 424 41. Held, I. M., Max, J. & Suarez, A. Proposal for the intercomparison of the dynamical
425 cores of atmospheric general circulation models. *Bull. Am. Meteorol. Soc.* **75**, 1825–
426 1830 (1994).
- 427 42. James, P. M., Fraedrich, K. & James, I. N. Wave-zonal-flow interaction and ultra-low
428 frequency variability in a simplified global circulation model. *Q. J. R. Meteorol. Soc.*
429 **120**, 1045–1067 (1994).
- 430 43. Yoo, C., Lee, S. & Feldstein, S. B. Arctic response to an MJO-like tropical heating in
431 an idealized GCM. *J. Atmos. Sci.* **69**, 2379–2393 (2012).
- 432

432 **Statement of correspondence author**

433 Correspondence and requests for materials should be addressed to Xichen Li and Shang-

434 Ping Xie.

435

435 **Acknowledgements**

436 X.L. was supported by the Scripps Postdoctoral Fellowship; S.-P.X. was
437 supported by the NSF grant AGS-1305719; S.T.G. was supported by the NSF grant OCE-
438 1234473. C.Y. was supported by the Korea Meteorological Administration Research
439 and Development Program under Grant KMIPA 2015-6110.

440 The HadISST sea surface temperature (SST) data were provided by the British
441 Met Office, Hadley Centre. The Kaplan SST and ERSST data sets were provided by the
442 National Oceanic and Atmospheric Administration (NOAA) Earth System Research
443 Laboratory. The Global Precipitation Climatology Project (GPCP) data were provided by
444 the World Climate Research Programme's (WCRP) Global Energy and Water Exchanges
445 Projects (GEWEX). Ishii subsurface temperature data were provided by the National
446 Center for Atmospheric Research (NCAR) CISL Data Research Archive. The ERA-
447 Interim atmospheric reanalysis was provided by the European Centre for Medium Range
448 Weather Forecasts (ECMWF). We thank the WCRP Working Group on Coupled
449 Modelling, which is responsible for CMIP multi-model ensemble. The community earth
450 system model, CESM, and its atmospheric component, CAM4, were made available by
451 NCAR, supported by the National Science Foundation (NSF) and the Office of Science
452 of (BER) the U.S. Department of Energy (DOE). The idealized atmospheric model,
453 GFDL dry-dynamical-core, was developed by the NOAA at the Geophysical Fluid
454 Dynamics Laboratory (GFDL).

455 Computing resources were provided by the Yellowstone high-performance
456 computing (HPC) in NCAR's Computational and Information Systems Laboratory, and
457 by the HPC at New York University (NYU).

458

458 **Author Contributions**

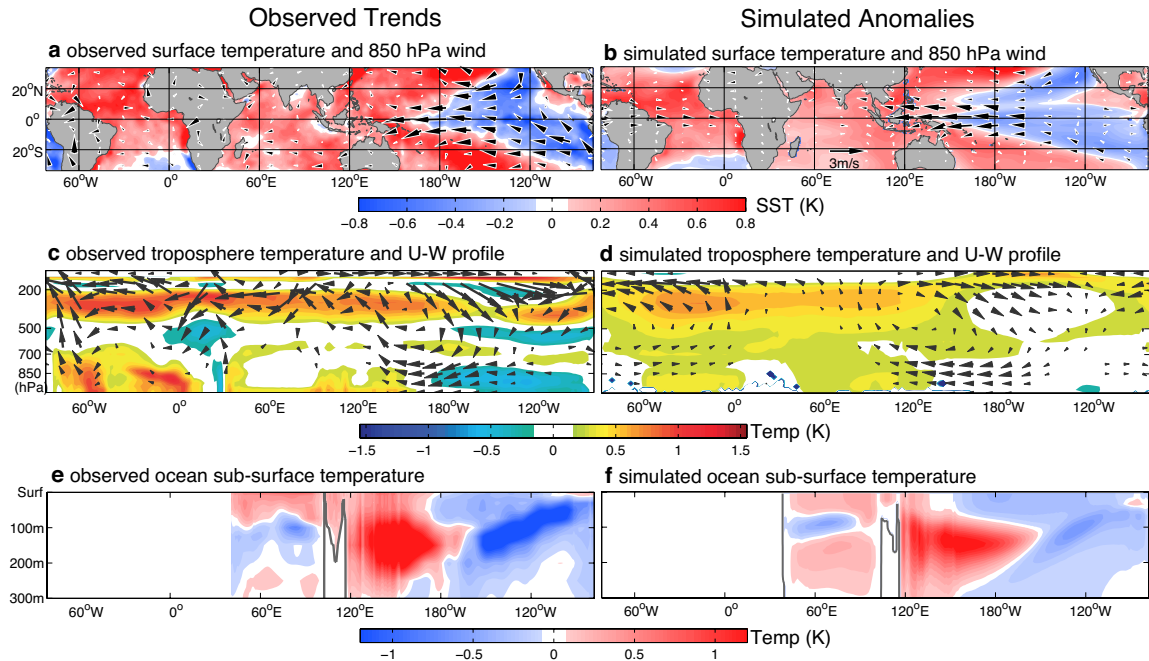
459 X.L., S.-P.X. and S.T.G. designed the experiments; X.L. performed the data analysis and
460 numerical simulations, and prepared all figures; X.L. and C.Y. ran the CESM and GFDL
461 simulations; all authors wrote and reviewed the manuscript.

462

462 **Competing Financial Interest:**

463 The authors declare no competing financial interests.

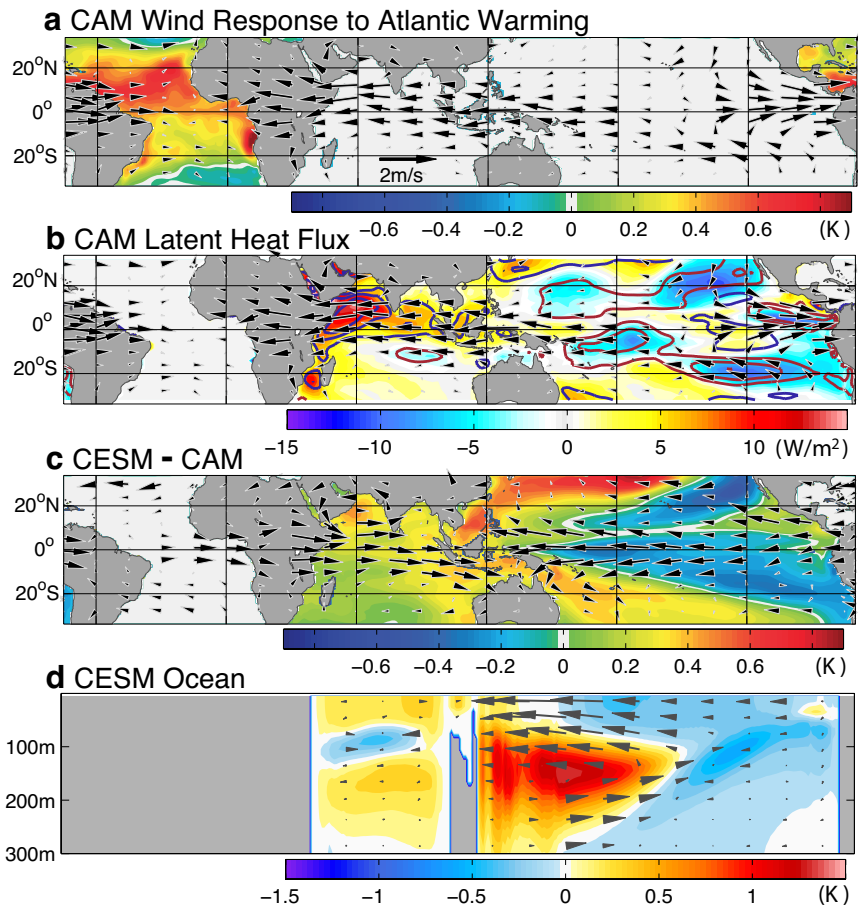
464



465

466 **Figure 1 | Observed tropical climate changes (a, c, e) can be well reproduced by the**
 467 **CESM coupled model simulation (b, d, f), forced by the observed tropical-Atlantic-**
 468 **only SST changes.** The (a) observed and (b) simulated sea surface temperature (SST)
 469 changes (background color) and 850hPa wind anomaly (arrows) both exhibit a pan-
 470 tropical dipole SST change, with warming extending from the Tropical Atlantic to the
 471 Indian Ocean and the Western Pacific, and cooling over the Central-Eastern Pacific. The
 472 observed trends (a) are estimated using the Sen's slope method, from 1979 to 2012. c and
 473 d show the Walker circulation changes (arrows) and troposphere temperature anomalies
 474 (color shading): the Indo-Pacific Walker circulation is enhanced. The vertical velocity is
 475 magnified by a factor of 750 to make its scale comparable to that of zonal wind. The (e)
 476 observed and (f) simulated ocean subsurface temperature anomalies (color shading) are
 477 shown for the tropical cross section between 5°S – 5°N.

478



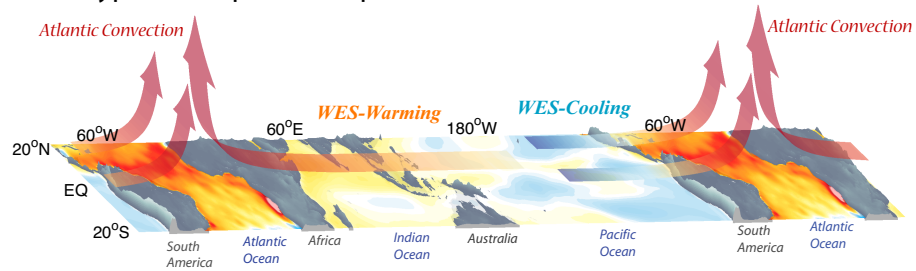
478

479 **Figure 2 | Physical pathway for the Atlantic warming to drive tropical wide SST**
 480 **changes. a.** shows the Atlantic SST forcing and 850hPa wind responses in CAM4. Deep
 481 convection forced by the tropical Atlantic warming induces convergent flows over the
 482 entire tropical region, i.e. easterly wind anomalies over the Indo-Western Pacific and
 483 westerly wind anomalies over the Eastern Pacific. **b.** The wind changes in CAM4 further
 484 reduce the surface wind speed (blue contours) over vast areas of the Indian Ocean,
 485 suppress evaporation, and thus reduce the latent heat flux (red/yellow shading) from the
 486 ocean to the atmosphere (equivalent to a heating in the ocean). They also increase the
 487 surface wind speed (red contours) over much of the off-equatorial Eastern Pacific and
 488 thus increase latent heat flux (blue shading) there. **c.** CESM - CAM4 differences in SST
 489 and 850hPa wind. The anomalous Atlantic warming heats the Indo-Western Pacific and
 490 cools the Eastern Pacific. This SST gradient generates a secondary atmospheric

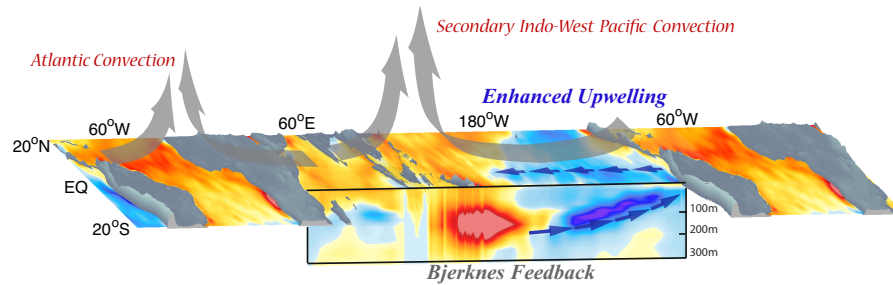
491 circulation change, characterized by an enhanced easterly wind anomaly over the Pacific,
492 and a westerly wind anomaly over the Atlantic-Indian Oceans. **d.** sub-surface temperature
493 and ocean current responses in CESM (the vertical velocity is magnified by 4000 times).
494 The easterly wind anomaly further drives the ocean surface current, strengthens the
495 equatorial undercurrent and generates a La Niña-like ocean dynamical response.
496 Processes shown in **c** and **d** interact with each other through the Bjerknes feedback.

497

a Gill-type Atmospheric Response and WES Effect



b Gill-type Atmospheric Response and Bjerknes Feedback



497

498 **Figure 3 | Schematic graph of the physical mechanism. a** Atlantic warming generates
499 anomalous atmospheric deep convection, mimicking the Gill-convective-model²⁸. The
500 deep convection forces an easterly wind anomaly over the Indian Ocean that suppresses
501 local evaporation and increases the SST there. This is accompanied by a Rossby-wave
502 induced wind anomaly of opposing sign, which cools the Eastern Pacific. This
503 atmosphere-ocean surface interaction initiates a temperature gradient over the Indo-
504 Pacific oceans. **b** the Pacific ocean dynamic effect positively feeds back on this SST
505 gradient, i.e. the SST gradient generates a secondary deep convection over Indo-Western
506 Pacific warm pool, reinforcing the easterly wind anomalies over the Pacific basin, which
507 intensifies the Ekman pumping over the Eastern Pacific and enhances the Pacific
508 undercurrent. These dynamical effects cool the Eastern Pacific and warm the Western
509 Pacific, forming a positive feedback. The vertical cross-section in **b** illustrates the
510 temperature and circulation anomalies in the sub-surface Indo-Pacific.

511

512

513

513 **Atlantic Induced Pan-tropical Climate Change over the Past Three Decades**

514 **Supplementary Information**

515 **POP simulation forced by the Atlantic-induced atmospheric circulation changes.**

516 The Atlantic induced atmospheric circulation changes involve an easterly wind anomaly
517 over the Indo-Western Pacific and a westerly wind anomaly over the eastern equatorial
518 Pacific. The former favors a La-Niña-type ocean dynamical response, while the latter
519 favors an El-Niño-type response. To investigate the direct impact of the atmospheric
520 circulation anomalies to the Indian Ocean and the Pacific, we perform an additional
521 simulation using an ocean-only model (POP2, the oceanic component of the CESM
522 model), forced by the Atlantic induced surface wind anomalies from CAM4 (**Fig. 2a**).

523 The SST anomaly patterns (**Supplementary Fig. 6a**) are similar to the latent heat
524 flux anomalies (**Fig. 2b**), especially since both figures show cooling signals over the off-
525 equatorial Pacific and the central equatorial Pacific, as well as warming anomalies over
526 most of the Indian Ocean. These highlight the dominant effect of the WES forcing prior
527 to the Bjerknes feedback.

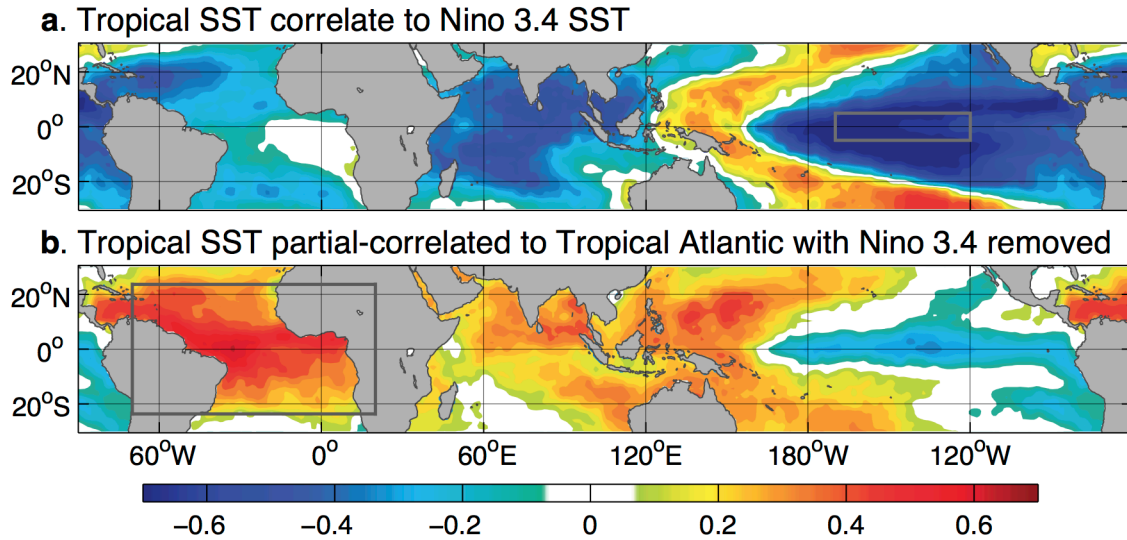
528 There are two differences between the SST pattern and the latent heat flux
529 pattern: 1) the warming SST anomaly over the eastern equatorial Pacific, and 2) the
530 strengthened cooling SST anomaly over the southeastern Indian Ocean, both of which are
531 related to the oceanic dynamical response. The former is forced by the westerly wind
532 anomaly over the eastern equatorial Pacific (**Fig. 2a**), while the latter can be explained by
533 the easterly wind anomaly over the Indian Ocean. These phenomena are also seen in the
534 subsurface anomalies (**Supplementary Fig. 6b**): the thermocline shoals in the central
535 equatorial Pacific but deepens in the eastern Pacific, while on the east coast of the Indian
536 Ocean we see a narrow upwelling.

537 Note that the POP simulation results illustrate only the direct ocean response to
538 atmospheric circulation changes, prior to any ocean-atmosphere feedbacks. We find the
539 simulation results with an active ocean-atmosphere feedback to be different from this
540 ocean-only model result. As shown in the main text, the temperature gradient over the
541 Indo-Pacific basin enhances the Walker circulation. The Bjerknes feedback triggered by
542 the easterly wind anomaly over the Pacific basin further cools the eastern equatorial
543 Pacific and warms the southeastern Indian Ocean, leading to the observed SST changes.

544

545 **Robustness of the tropical-wide SST pattern.** We check the robustness of the model
546 response to the observed Tropical Atlantic warming, by performing two additional
547 sensitivity experiments forced by the Atlantic forcing scaled to 80% and 120% of the
548 observed SST trend, respectively. The simulation results (**Supplementary Fig. 10**) are
549 then compared with the results of the original experiment driven by the observed trend.
550 While the amplitudes of the model responses vary with the intensity of the Tropical
551 Atlantic forcing, all three experiments show a similar response to the external forcing,
552 indicating a pan-tropical SST anomaly, with enhanced easterly wind anomalies around
553 the equatorial Pacific region, which largely resemble the observed trends. These results
554 further confirm the robust relationship between the tropical Atlantic and the entire
555 Tropical Ocean, although many other characteristics of this teleconnection, such as the
556 linearity, require additional investigation. These will be the subject of our future research.

557



558

559 **Supplementary Figure 1 | 3-month lagged correlation (lagged partial correlation)**

560 **between tropical SST and Eastern Pacific (Tropical Atlantic). a** 3-month lagged-

561 correlation coefficients with the Niño3.4 time series, based on 1870-2012 HadISST

562 datasets. The global warming trend was removed. All correlation coefficients are

563 multiplied by -1. An Eastern Pacific cooling cools the Indian Ocean and the Tropical

564 Atlantic, opposite to the observed SST trend for 1979-2012. **b** the lagged-partial-

565 correlation coefficients with tropical Atlantic SST time series. The global warming trend

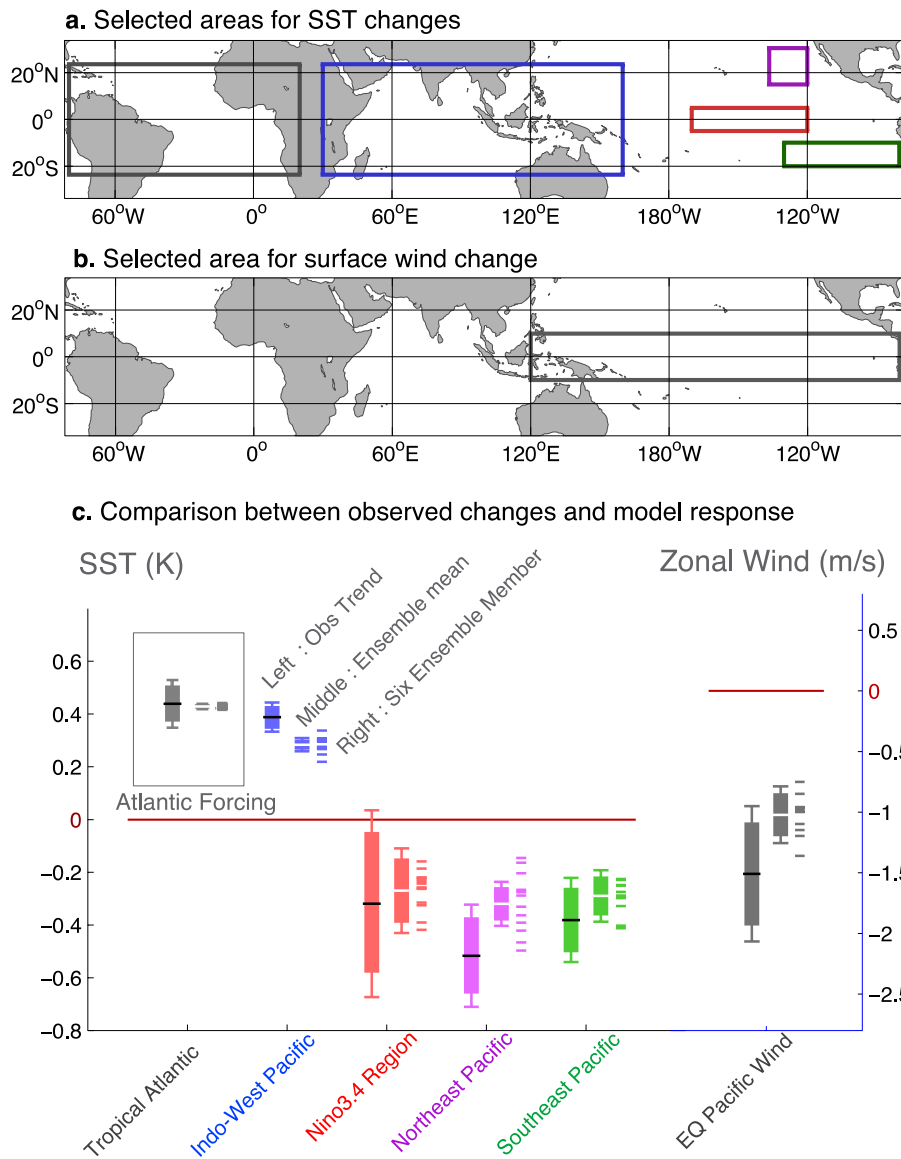
566 and the Niño3.4 variability were removed. A tropical Atlantic warming leads to an SST

567 anomaly, which closely resembles the observed SST trend for 1979-2012 and the CESM

568 simulation results, with warming over the Indo-Western Pacific and cooling over the

569 Central-Eastern Pacific.

570



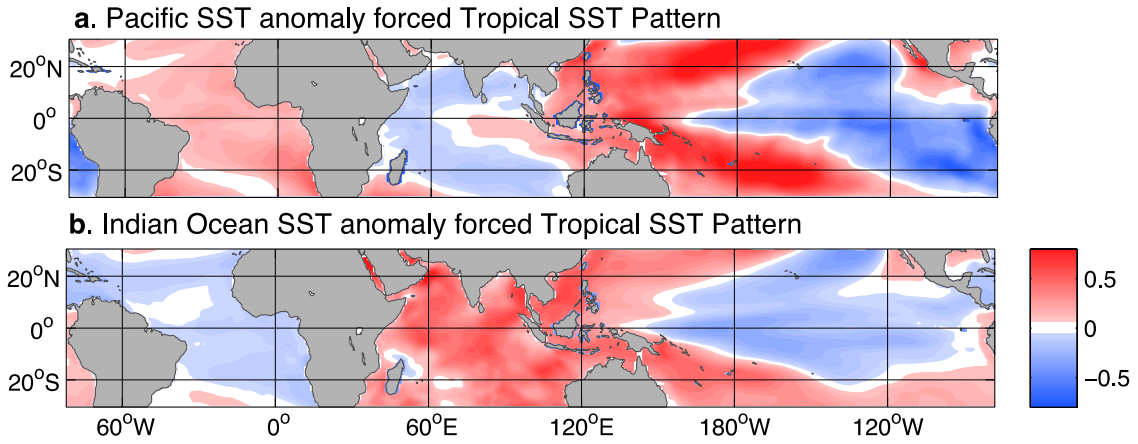
570

571 **Supplementary Figure 2 | Magnitudes and confidence intervals of the observed and**
 572 **simulated SST changes over five tropical regions, and easterly wind anomalies over**
 573 **the equatorial Pacific.** Panel **a** shows the five SST regions: the tropical Atlantic (grey),
 574 Indo-Western Pacific (blue), Niño 3.4 area (red), off-equatorial Northeastern Pacific
 575 (purple), and off-equatorial Southeastern Pacific (green). Panel **b** shows the equatorial
 576 Pacific region over which the zonal average is used to define the zonal wind index. Panel
 577 **c** shows the statistical analysis results. The observed changes over 1979-2012 are
 578 indicated by bars centered with black lines. The simulated changes are centered with
 579 white lines instead, with the model results of each of the 12 ensemble members marked

580 as short horizontal bars on the right. The thick vertical bars show the 95% confidence
581 intervals of these SST changes, and thin error bars indicate 99% confidence intervals.
582 The SST restoring in the model captures 97% of the observed Atlantic SST trends.
583 Results over the other regions capture about 55%~85% of the observed change.

584

584

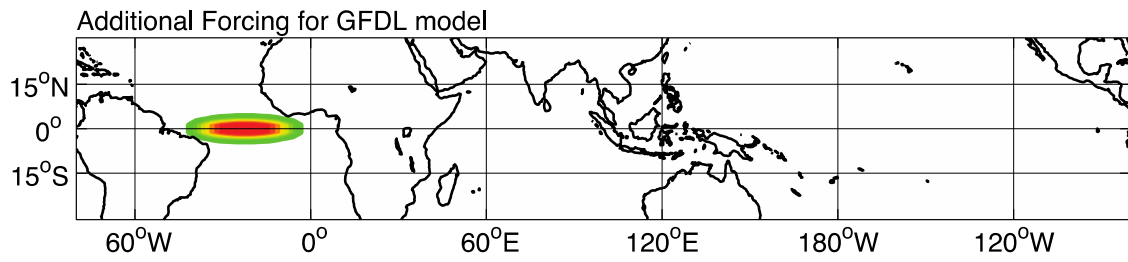


585

586

587 **Supplementary Figure 3 | Sea surface temperature (SST) patterns forced by the**
588 **Pacific (upper panel) and Indian Ocean (lower panel) SST changes, simulated in the**
589 **coupled model.**

590

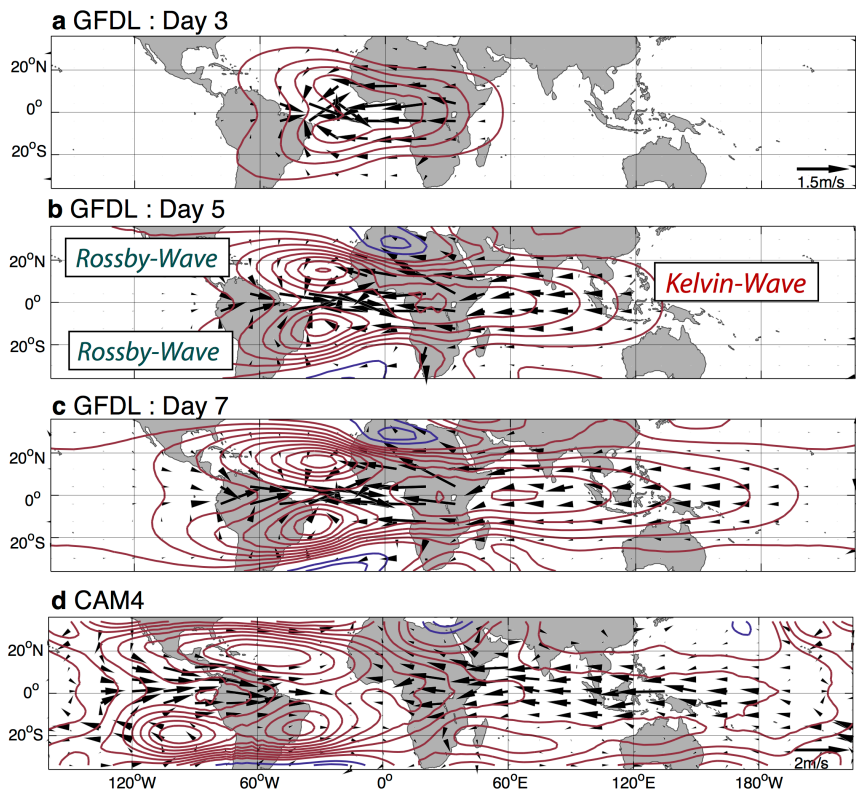


590

591 **Supplementary Figure 4 | The horizontal structure of the external forcing in the**

592 **GFDL atmospheric dynamical-core.**

593

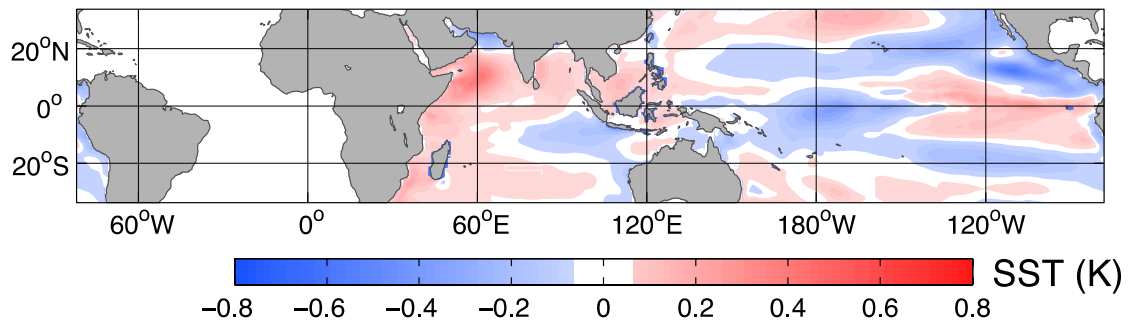


593

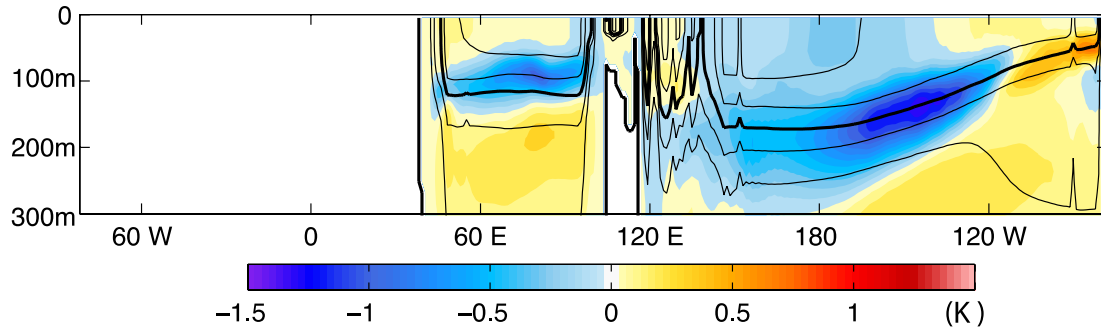
594 **Supplementary Figure 5 | Atlantic warming induced atmospheric circulation**
 595 **changes, simulated by GFDL dynamical-core and CAM4.** a to c show the GFDL
 596 simulated 850hPa wind (vectors) and 200hPa geopotential height (contours) anomalies on
 597 day 3, day 5, and day 7 respectively, after initiating an external heating mimicking the
 598 tropical Atlantic warming. The Atlantic heating first generates deep convection (a),
 599 which further forms a classic Gill-type pattern²⁵ (b). The Kelvin-wave-induced easterly
 600 wind anomalies extend from the Atlantic to the Indian Ocean and to the Central-Western
 601 Pacific within a week (c), while the two Rossby wave packets occupy the central
 602 America and the Eastern Pacific with equatorial westerly wind anomalies. The CAM4
 603 simulation (d) results agree with those from the dry GFDL idealized model (c), although
 604 the southern packet of the Rossby wave is interrupted by topography.

605

a. POP SST response to the Atlantic induced Gill-type Circulation Changes



b. POP subsurface response to the Atlantic induced Gill-type Circulation Changes



605

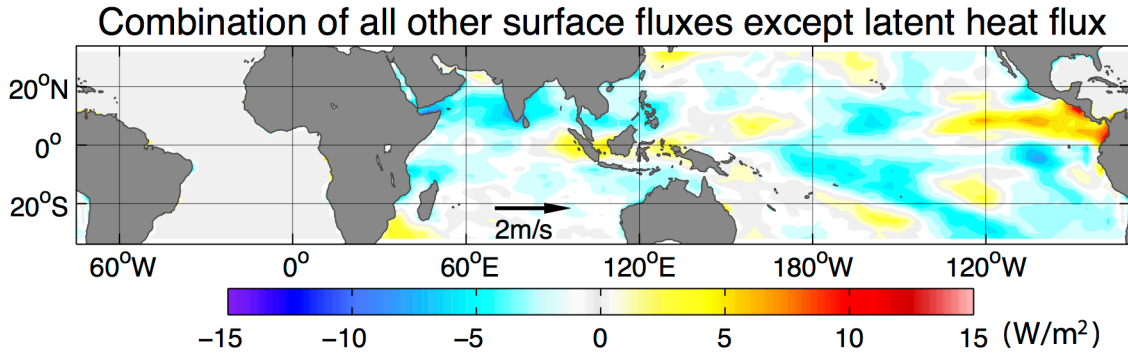
606 **Supplementary Figure 6 | Ocean model responds to the Atlantic warming induced**

607 **atmospheric circulation changes. a shows the SST responses, and b shows the sub-**

608 **surface temperature responses.**

609

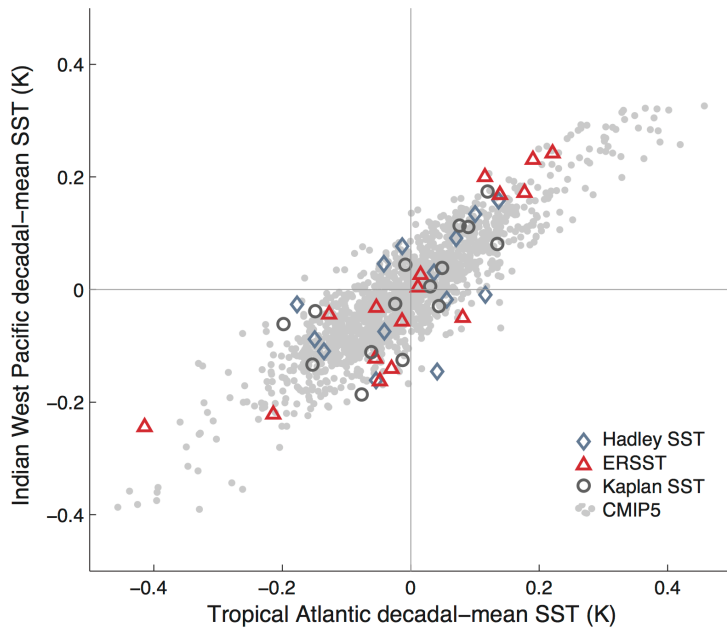
609



610

611 **Supplementary Figure 7 | The combined anomalies of atmosphere-ocean sensible**
612 **heat flux, solar radiation and long wave radiation in CAM4.** These three terms
613 combined have a weaker effect than the latent heat anomaly induced by the Atlantic
614 warming (see **Figure 2b**).

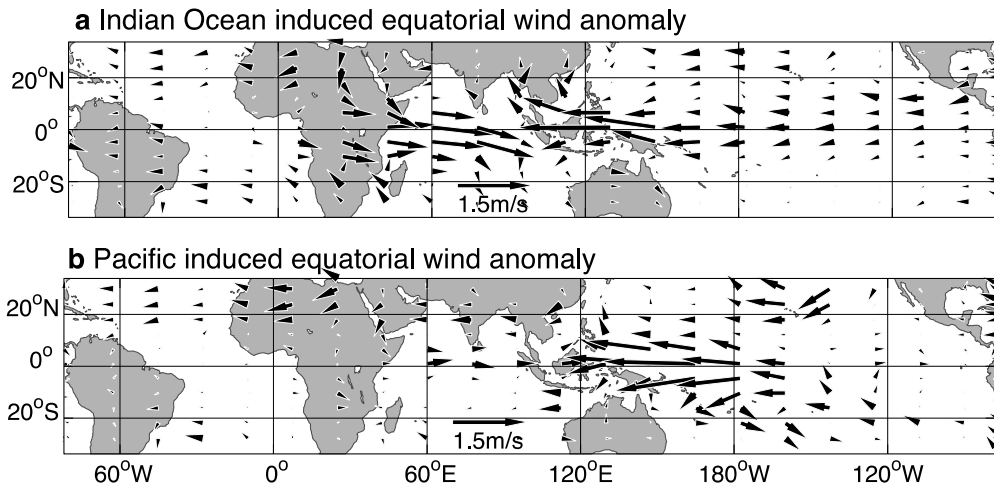
615



615

616 **Supplementary Figure 8 | Relationship between the decadal mean sea surface**
 617 **temperature (SST) of the Tropical Atlantic and Indo-Western Pacific in**
 618 **observations and unforced historical CMIP5 simulations from 1850 until the**
 619 **present.** The long-term global warming trends are removed from each dataset. In both
 620 observations (colored symbols) and CMIP simulations (grey dots), the Tropical Indo-
 621 Western Pacific SST tightly co-varies with the Tropical Atlantic SST.

622



622

623 **Supplementary Figure 9 | Wind anomaly in CAM4, forced by the Atlantic-induced**

624 **Indian Ocean and Pacific SST changes, separately.** Both SST forcing terms drive

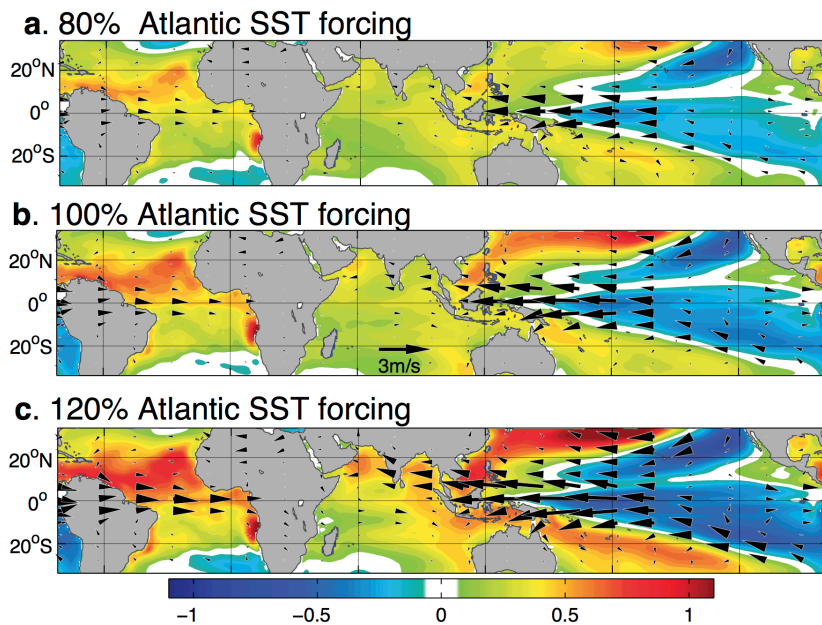
625 easterly wind anomalies over the equatorial Pacific. The Indian-Ocean-induced easterly

626 wind anomaly occupies the entire equatorial Pacific, while the Pacific-induced wind

627 anomaly is part of the Bjerknes feedback. The easterly wind induced by Pacific SST

628 changes is strong over the Western Pacific and is weaker over the Eastern Pacific.

629



629

630 **Supplementary Figure 10 | Tropical SST and 850hPa wind anomalies responding to**
 631 **the Tropical Atlantic warming of different amplitudes.** Panels a – c show the CESM
 632 simulation results forced by the Tropical Atlantic warming with 80%, 100%, and 120%
 633 of the observed trend, respectively. In all cases, the Tropical Atlantic warming drives
 634 similar tropical-wide SST and lower-troposphere wind patterns, resembling the observed
 635 trend during the last three decades, although the amplitudes of the model responses vary
 636 with the strength of the Atlantic forcing.

637